Brazilian Journal of Geophysics, 40 (2022), Suppl. 1, 7–19
Brazilian Geophysical Society
ISSN 2764-8044
DOI: 10.22564/brjg.v40i5.2139

3D DISPLACEMENT AND STRESS FIELDS OF COMPACTING RESERVOIR: ALTERNATIVE SOLUTIONS

Valeria C. F. Barbosa [1*], Vanderlei C. Oliveira Jr [1], Andre D. Arelaro [2], and Filipe Augusto S. Borges [2]

[1]Observatório Nacional - ON, Rio de Janeiro, RJ, Brazil
[2]Petróleo Brasileiro S.A. - Petrobras, Rio de Janeiro, RJ, Brazil

Corresponding author e-mail: valcris@on.br

ABSTRACT. We have presented alternative solutions for the displacement and stress fields outside and inside of a 3D right rectangular prism under constant pressure. These solutions are obtained by integrating the well-known nucleus-of-strain solution over the volume of the prism. They are based on the similarity between the gravitational potential yielded by a volume source under a density variation and the thermoelastic displacement potential yielded by a volume source in a half-space under a pressure variation. This similarity enables the use of closed expressions of the gravitational potential and its derivatives. We use our solution for approximating the displacement and stress fields due to a reservoir with an arbitrary shape and under arbitrary pressure changes. We discretized the reservoir as a grid of 3D right rectangular prisms juxtaposed in the horizontal and vertical directions. Each prism has homogeneous pressure; however, pressure variations among different prisms are allowed. This parametrization of the reservoir yields a piecewise constant distribution of pressure in the subsurface. We validate the resultant displacement and stress fields due to the reservoir by numerical simulations including a reservoir with arbitrary geometry and under arbitrary pressure distribution, based on a production oil field in offshore Brazil.

Keywords: gravitational potential, reservoir compaction, hydrocarbon production, nucleus-of-strain solution, mathematical and numerical modeling

INTRODUCTION

The surface subsidence due to oil or gas withdrawal from a reservoir in the subsurface may occur as a result of geomechanical changes caused by pressure drop. The phenomenon of subsidence by fluid extraction has been observed in a variety of oil fields, e.g., the Ekofisk field, southern North Sea (Borges et al., 2020) and the Groningen gas field in the northeast Netherlands (van Thienen-Visser and Fokker, 2017). As the subsidence close to hydrocarbon fields under production can induce earthquakes (Dahm et al., 2015; Grigoli et al., 2017), the petroleum companies have had an increased interest in monitoring the magnitude and distribution of subsidence resulting from reservoir depletion. This monitoring is accomplished by means of the numerical modeling of the displacement field. The physical foundation of the displacement, stress and strain fields in the subsurface due to a reduction of pressure in the reservoir comes from the theory of thermoelasticity. In the uncoupled thermoelasticity theory for quasi-static problems (i.e., problems with negligible inertia effects), Goodiee (1937) employed the method of superposition using displacement potential functions and introduced the concept of nucleus of thermoelastic strain in an infinite space. Specifically, Goodiee's method (1937) simplified the thermoelastic problem by replacing it with an isothermal elastic problem with different boundary conditions together with the solution of a Poisson's equation (Tao, 1971). Mindlin and Cheng (1950) and Sen (1951) extended Goodiee's method to a homogeneous half-space. Sharma (1956) deduced the displacement and stress fields in an infinite elastic plate due to a nucleus of thermoelastic strain located at a point inside it by using infinite integrals involving Bessel functions.

The subsidence resulting from reservoir depletion is in the context of poroelastic theory. Geertsma (1957) remarked on the analogy between the theories of thermoelasticity and poroelasticity. To our knowledge, Geertsma (1973) was the first to solve the poroelastic problem by using the nucleus-of-strain concept in the half-space, which in turn was proposed by Mindlin and Cheng (1950) and Sen (1951) in the theory of thermoelasticity. Geertsma's approach presumes that the total displacement field due to the compaction of a compacting region in the subsurface is the superposition of the displacement field due to its constituting points. Each constituting point, in turn, is represented by a small sphere called the nucleus of strain. By using this idea, Geertsma (1973) derived analytical expressions by integrating the nucleus-of-strain solution over the volume of a thin disk-shaped reservoir. Segall (1992) followed Geertsma (1973) and extended the analytical solutions of the displacement and stress fields assuming general axisymmetric geometries and an arbitrary radial pressure distribution. Geertsma and van Opstal (1973) applied the nucleus-of-strain concept in the half-space to calculate the spatial subsidence distribution due to the production of the reservoir with an arbitrary 3D shape. By assuming a producing reservoir embedded in a homogeneous, isotropic, and elastic medium, and a reservoir model in which the pressure perturbations are related to the displacement field by a linear relationship, Geertsma and van Opstal (1973) (1973) discretized the reservoir into a grid of nuclei-of-strain and calculated the displacement due to the pressure change in the whole reservoir by the superposition of the displacement due to the constant pressure change in each nucleus. Tempone et al. (2010) followed Geertsma and van Opstal (1973) and extended the nucleus-of-strain concept in the half-space to consider the effects of a rigid basement. The main drawbacks in Geertsma and van Opstal (1973) and Tempone et al. (2010) are the assumption of a homogeneous reservoir and the fact that the solution is only valid outside the reservoir. In this case, the displacements within the reservoir are calculated by linear interpolation of the displacements at the upper and lower edges of the reservoir Tempone et al. (2012). Considering an inhomogeneous poroelastic model that consists of layered stratigraphy, Mehrabian and Abousleiman (2015) developed closed-form formulae for the displacement and stress fields outside and inside of the reservoir embedded within elastic strata with different mechanical properties and subjected to pore pressure disturbances due to fluid extraction or injection. Muñoz and Roehl (2017) assume a linear elastic semi-infinite medium to develop an analytical solution for the displacement field outside and inside of a rectangular prism having a constant pressure change. Their approach consists in integrating the Geertsma's nucleus-of-strain solution over the volume of the prism. Then, they discretize an arbitrarily-shaped reservoir under an arbitrary distribution of pressure changes into a grid of prisms having different constant pressure changes. Finally, they compute the total displacement field outside and inside of the reservoir by adding the displacement fields produced by all prisms setting up the reservoir model.

The present work assumes a linear elastic semi-infinite medium and provides an alternative solution for the displacement field outside and inside of a rectangular prism with constant pressure change. Like Muñoz and Roehl (2017), we integrate the Geertsma's nucleus of strain over the prism volume. We also use our alternative solution to approximate the displacement field due to an arbitrarily-shaped reservoir under arbitrary pressure changes by the superposition of the displacement fields produced by a grid of prisms. Like Vasco and Johnson (1987), we take advantage of the similarity between the equations for calculating the displacement field due to a volume source in a half-space under a pressure variation and the gravitational potential due to a volume source under a density variation. In contrast with Vasco and Johnson (1987), our approach calculates the displacement field due to a 3D volume source at the whole subsurface whereas Vasco and Johnson (1987) calculated the displacement field due to a 2D volume source at the Earth's surface. We use closed expressions of the gravitational potential and its derivatives produced by the 3D right rectangular prism derived by Nagy et al. (2000, 2002) and Fukushima (2020) for calculating the displacement field due to a 3D prism under a constant pressure variation.

THEORY

The displacement, stress, and strain fields in the subsurface caused by reservoir compactation due to hydrocarbon production are grounded on the theory of thermoelasticity. The Goodiee's thermoelastic displacement potential ϕ satisfies the Poisson's equation (Goodiee, 1937), i.e.:

$$\nabla^2 \phi = m\, T, \tag{1}$$

where ∇^2 is the Laplacian operator, T is the temperature variation and $m = \alpha \frac{1+\nu}{1-\nu}$, where α is the coefficient of linear thermal expansion and ν is the Poisson's ratio. From the potential theory, a particular solution of Equation 1 is

$$\phi(x,y,z) = -\frac{m}{4\pi} \int\limits_{v}\int\int \frac{T(x',y',z')}{\sqrt{(x-x')^2+(y-y')^2+(z-z')^2}}\, dv', \tag{2}$$

where $\phi(x,y,z)$ represents the Newtonian gravitational potential (Kellogg, 1967) that would be produced at the coordinates x, y and z by a continuous density distribution $-\frac{m}{4\pi}\, T(x',y',z')$. The integral in

Equation 2 is conducted over the coordinates x',y' and z', denoting, respectively, the $x-$, $y-$ and $-z$ coordinates of an arbitrary point belonging to the interior of the volume v of the solid. From Equation 2 and the potential theory, Goodiee (1937) showed that, if an element of volume dv in the infinite solid is at a temperature $T(x', y', z')$, the remainder being at temperature zero, the displacement vector $\mathbf{u}$ caused by this temperature is the gradient of the Goodiee's thermoelastic displacement potential, i.e.,

$$\mathbf{u} = \nabla\phi(x, y, z) \,, \tag{3}$$

where ∇ is the gradient operator. To a homogeneous half-space, Mindlin and Cheng (1950) showed that the method proposed by Goodiee (1937) can be extended by the displacement solution given by:

$$\mathbf{u} = \nabla\,\phi_{\mathbf{1}} \;+\; \nabla_{\mathbf{2}}\phi_{\mathbf{2}}, \tag{4}$$

where $\phi_1 \equiv \phi_1(x, y, z)$ is the potential defined in Equation 2; $\phi_2 \equiv \phi_2(x, y, z)$ is defined as "image potential" (Segall, 1992) due to an image point at the coordinates $(x', y', -z')$; and the operator $\nabla_{\mathbf{2}}$ is

$$\nabla_{\mathbf{2}} = (3 - 4\nu)\nabla + 2\nabla z\frac{\partial}{\partial z} - 4(1 - \nu)\hat{\mathbf{z}}\nabla^{\mathbf{2}}_{\mathbf{z}}, \tag{5}$$

where $\hat{\mathbf{z}}$ is the unit vector in the $z-$direction and $\nabla^{\mathbf{2}}_{\mathbf{z}}$ is a scalar operator in which the operand is firstly multiplied by z and then operated upon by the Laplacian $\nabla^{\mathbf{2}}$. Equation 4 is the displacement solution for the variation of temperature due to a single nucleus of strain buried at depth z' in a semi-infinite homogeneous medium. In the right hand side of Equation 4, the first term $\nabla\,\phi_1$ represents the displacement in an infinite medium, and the second term represents a correction of the displacement due a half-space, also known as "image nucleus solution".

METHODOLOGY

Let's assume that a reservoir in the interior of the Earth is subject to a compaction due to hydrocarbon production. The compaction is caused by the pressure change within the reservoir, which in turn causes surface subsidence (or surface displacement). Here, we use a Cartesian coordinate system with the $x-$axis pointing to the north, the $y-$axis pointing to the east, and the $z-$axis pointing downward. We discretize the reservoir into an $m_x \times m_y \times m_z$ grid of 3D vertical juxtaposed prisms ($m_x{\cdot}m_y{\cdot}m_z = M$) along the x, y and z axes, respectively, in which the pressure within each prism is assumed to be constant and known. Each prism in the reservoir model may undergo a distinct pressure change. The subsidence effect is the displacement field due to the pressure change throughout the reservoir and is calculated by the sum of the displacement produced by each prism. The discrete forward modeling to calculate the displacement and stress fields due to a piecewise-constant distribution of the pressure variation within a reservoir follows the nucleus-of-strain approach. We assume that a nucleus of strain represents an infinitesimal reservoir volume element. The displacement solution for a single nucleus of strain in a homogeneous elastic semi-infinite medium (Equation 4) will be used as an element of the displacement. We calculate the displacement (stress) field due to the pressure variation of a prism by integrating the nucleus of strain over its volume.

The discrete forward modeling due to a nucleus of strain in a homogeneous elastic semi-infinite medium

By considering the discrete form of Equation 4, the displacement vector $\mathbf{u}_{ij} \equiv \mathbf{u}(x_i, y_i, z_i, x'_j, y'_j, z'_j)$ at an arbitrary point (x_i, y_i, z_i) due to a change of pressure in the jth nucleus of strain at the coordinates (x'_j, y'_j, z'_j) will be calculated by

$$\mathbf{u}_{ij} = \mathbf{u}_{\mathbf{1}ij} + \mathbf{u}_{\mathbf{2}ij} \,, \tag{6}$$

where $\mathbf{u}_{\mathbf{1}ij}$ is the displacement vector at the point (x_i, y_i, z_i) due to the jth single nucleus in the infinite space and $\mathbf{u}_{\mathbf{2}ij}$ is the correction of the displacement considering a semi-space (image nucleus solution). The term $\mathbf{u}_{\mathbf{1}ij}$ (Equation 6) is given by

$$\mathbf{u}_{\mathbf{1}ij} = A_E\,\nabla\left(\frac{1}{R_{1ij}}\right)\,\Delta p_j\;\,dv'_j \tag{7}$$

and represents the gradient of the potential

$$\phi_1 = -\frac{C_m}{4\pi}\frac{\Delta p_j\;\,dv'_j}{R_{1ij}} \,. \tag{8}$$

The term $\mathbf{u}_{\mathbf{2}ij}$ (Equation 6) is given by

$$\begin{aligned}\mathbf{u}_{\mathbf{2}ij} = A_E\Bigg[&C_\nu\,\nabla\left(\frac{1}{R_{2ij}}\right) + 2\nabla\left(z\frac{\partial}{\partial z}\frac{1}{R_{2ij}}\right)\\ &- 4(1-\nu)\hat{\mathbf{z}}\nabla^{\mathbf{2}}\left(\frac{z}{R_{2ij}}\right)\Bigg]\Delta p_j dv'_j\end{aligned} \tag{9}$$

and is obtained by applying the operator $\nabla_{\mathbf{2}}$ (Equation 5) to the image potential

$$\phi_2 = -\frac{C_m}{4\pi}\frac{\Delta p_j\;\,dv'_j}{R_{2ij}} \,. \tag{10}$$

In Equations (7) to (10), all derivatives are computed with respect to the coordinates of the point (x_i, y_i, z_i); Δp_j is the pressure change of the jth nucleus; dv'_j is an infinitesimal element of volume centered at the jth nucleus of strain (x'_j, y'_j, z'_j), $C_\nu = (3 - 4\nu)$, $A_E = \frac{A(1+\nu)}{E}$, where A is the constant

$$A = -\frac{C_m E}{4\pi(1 + \nu)} \,, \tag{11}$$

E is the Young's modulus and C_m is the uniaxial com-

paction coefficient (see Geertsma, 1966)

$$C_m = \frac{1}{E}\,\frac{(1+\nu)(1-2\nu)}{(1-\nu)}\,. \tag{12}$$

In Equation 8, R_{1ij} is the distance from the ith point (x_i, y_i, z_i) to the jth nucleus of strain (x'_j, y'_j, z'_j), i.e.: $R_{1ij} = \sqrt{(x_i - x'_j)^2 + (y_i - y'_j)^2 + (z_i - z'_j)^2}$. In Equation 10, R_{2ij} is the distance from the ith point (x_i, y_i, z_i) to the jth image nucleus $(x'_j, y'_j, -z'_j)$, i.e.: $R_{2ij} = \sqrt{(x_i - x'_j)^2 + (y_i - y'_j)^2 + (z_i + z'_j)^2}$. Figure 1 shows a schematic representation of the geometry of the nucleus-of-strain problem in a semi-infinite medium. The horizontal plane $z = 0$ is called the "free surface". The $x-$, $y-$ and $z-$components of the vectors $\mathbf{u_1}_{ij}$ (Equation 7) and $\mathbf{u_2}_{ij}$ (Equation 9) can be explicitly defined as follows:

$$\mathbf{u_1}_{ij} = A_E \begin{bmatrix} \frac{\partial}{\partial x}\frac{1}{R_{1ij}} \\ \frac{\partial}{\partial y}\frac{1}{R_{1ij}} \\ \frac{\partial}{\partial z}\frac{1}{R_{1ij}} \end{bmatrix} \Delta p_j\, dv'_j \tag{13}$$

and

$$\mathbf{u_2}_{ij} = A_E \left\{ C_\nu \begin{bmatrix} \frac{\partial}{\partial x}\frac{1}{R_{2ij}} \\ \frac{\partial}{\partial y}\frac{1}{R_{2ij}} \\ -\frac{\partial}{\partial z}\frac{1}{R_{2ij}} \end{bmatrix} + 2z_i \begin{bmatrix} \frac{\partial^2}{\partial x \partial z}\frac{1}{R_{2ij}} \\ \frac{\partial^2}{\partial y \partial z}\frac{1}{R_{2ij}} \\ \frac{\partial^2}{\partial z^2}\frac{1}{R_{2ij}} \end{bmatrix} \right\} \Delta p_j dv'_j. \tag{14}$$

By following Sharma (1956) and Tempone et al. (2010), the stress vector $\boldsymbol{\sigma}_{ij} \equiv \boldsymbol{\sigma}(x_i, y_i, z_i, x'_j, y'_j, z'_j)$ at the point (x_i, y_i, z_i) due to the jth single nucleus of strain buried in the half-space is given by

$$\boldsymbol{\sigma}_{ij} = \boldsymbol{\sigma}_{\mathbf{1}ij} + \boldsymbol{\sigma}_{\mathbf{2}ij}\,, \tag{15}$$

where $\boldsymbol{\sigma}_{\mathbf{1}ij} \equiv \boldsymbol{\sigma}_{\mathbf{1}}(x_i, y_i, z_i, x'_j, y'_j, z'_j)$ is the stress vector at the point (x_i, y_i, z_i) due to the jth single nucleus in the infinite space and $\boldsymbol{\sigma}_{\mathbf{2}ij} \equiv \boldsymbol{\sigma}_{\mathbf{2}}(x_i, y_i, z_i, x'_j, y'_j, z'_j)$ is the stress vector at the point (x_i, y_i, z_i) that gives the correction of the stress due to the jth image nucleus considering a semi-space. These two vectors are given by

$$\boldsymbol{\sigma}_{\mathbf{1}ij} = A \begin{bmatrix} \frac{\partial^2}{\partial x \partial z}\frac{1}{R_{1ij}} \\ \frac{\partial^2}{\partial y \partial z}\frac{1}{R_{1ij}} \\ \frac{\partial^2}{\partial z^2}\frac{1}{R_{1ij}} \end{bmatrix} \Delta p_j dv'_j, \tag{16}$$

and

$$\boldsymbol{\sigma}_{\mathbf{2}ij} = A \left\{ \begin{bmatrix} \frac{\partial^2}{\partial x \partial z}\frac{1}{R_{2ij}} \\ \frac{\partial^2}{\partial y \partial z}\frac{1}{R_{2ij}} \\ -\frac{\partial^2}{\partial z^2}\frac{1}{R_{2ij}} \end{bmatrix} + 2z_i \begin{bmatrix} \frac{\partial^3}{\partial x \partial z^2}\frac{1}{R_{2ij}} \\ \frac{\partial^3}{\partial y \partial z^2}\frac{1}{R_{2ij}} \\ \frac{\partial^3}{\partial z^3}\frac{1}{R_{2ij}} \end{bmatrix} \right\} \Delta p_j dv'_j. \tag{17}$$

According to Sharma (1956) and Tempone et al. (2010), the Beltrami's equations (Beltrami, 1920) and the equilibrium equations must be satisfied to obtain the contribution of the stress field in the half-space. Additionally, the boundary condition $\boldsymbol{\sigma}_{ij} = \mathbf{0}$ (Equation 15), where $\mathbf{0}$ is the zero vector, must be satisfied at the free surface ($z_i = 0$). This condition can be easily verified by adding the vectors $\boldsymbol{\sigma}_{\mathbf{1}ij}$ (Equation 16) and $\boldsymbol{\sigma}_{\mathbf{2}ij}$ (Equation 17) computed at any point on the free surface $(x_i, y_i, z_i = 0)$.

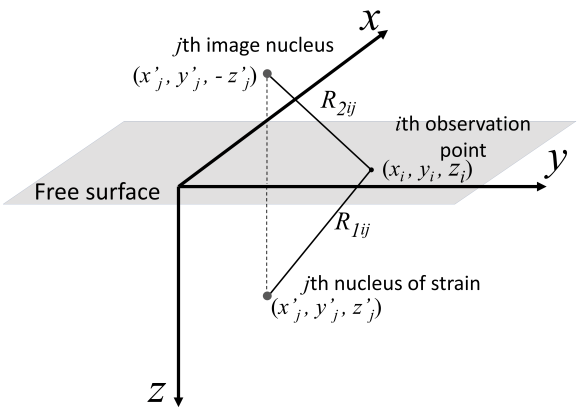

Figure 1: Schematic representation of the geometry of the nucleus of strain in a semi-infinite medium. After Muñoz and Roehl (2017). The adopted Cartesian coordinate system considered the $x-$axis pointing to the north, the $y-$axis pointing to the east, and the $z-$axis pointing downward.

The discrete displacement forward modeling due to a reservoir in a homogeneous elastic semi-infinite medium

We parameterize the reservoir as a grid of juxtaposed right rectangular prisms. Each grid prism undergoes a constant pressure change Δp_j; however, Δp_j can be different for every prism. To calculate the displacement field produced by the jth prism at the ith coordinates (x_i, y_i, z_i), we integrate the solution deduced for a single nucleus of strain (Equation 6) over its volume and obtain

$$\tilde{\mathbf{u}}_{ij} = \iiint_{v_{1j}} \mathbf{u_1}_{ij} dv'_j + \iiint_{v_{2j}} \mathbf{u_2}_{ij}\; dv'_j, \tag{18}$$

where both integrals are conducted with respect to the variables (x'_j, y'_j, z'_j). The first integral in Equation 18 is conducted over the volume v_{1j} of the jth prism and the second is conducted over the volume v_{2j} of a different prism symmetrically positioned above the free surface and conveniently called jth "image prism". The volume v_{1j} is defined by x_{1j}, x_{2j}, y_{1j}, y_{2j}, z_{1j}, and z_{2j}, which represent, respectively, the south, north, west, east, top, and bottom borders of the jth prism. The volume v_{2j} of the jth

image prism is defined in a similar way, but with top and bottom given by $z_{1j}-2\,z_{cj}$ and $z_{2j}-2\,z_{cj}$, where $z_{cj}=\frac{1}{2}(z_{1j}+z_{2j})$ is the center depth of the jth prism. The total displacement vector at the point (x_i, y_i, z_i) due to the pressure change in the whole reservoir is defined as the sum of the displacements $\mathbf{u}_{ij}$ (Equation 18) yielded by each prism with constant pressure Δp_j:

$$\tilde{\mathbf{u}}_i = \sum_{j=1}^{M} \tilde{\mathbf{u}}_{ij}, \tag{19}$$

where M is the number of prisms setting up the reservoir model. The horizontal component of the total displacement vector $\tilde{\mathbf{u}}_i$ (Equation 19) is calculated by

$$\tilde{u}_{i_h} = \sqrt{\tilde{u}_{i_x}^2 + \tilde{u}_{i_y}^2}, \tag{20}$$

where $\tilde{u}_{i_x}$ and $\tilde{u}_{i_y}$ are the $x-$ and $y-$ components. By substituting Equation 13 and Equation 14 into Equation 18, we obtain

$$\begin{aligned}\tilde{u}_{ij_\alpha} = A_E \Delta p_j \Bigg[&\iiint_{v_{1j}} \frac{\partial}{\partial\alpha}\frac{1}{R_{1ij}} dv'_j + \\ &C_\nu \iiint_{v_{2j}} \frac{\partial}{\partial\alpha}\frac{1}{R_{2ij}} dv_j + \\ &2z_i \iiint_{v_{2j}} \frac{\partial^2}{\partial\alpha\partial z}\frac{1}{R_{2ij}} dv'_j \Bigg],\end{aligned} \tag{21}$$

where $\alpha = x, y$, and

$$\begin{aligned}\tilde{u}_{ij_z} = A_E \Delta p_j \Bigg[&\iiint_{v_{1j}} \frac{\partial}{\partial z}\frac{1}{R_{1ij}} dv'_j - \\ &C_\nu \iiint_{v_{2j}} \frac{\partial}{\partial z}\frac{1}{R_{2ij}} dv'_j + \\ &2z_i \iiint_{v_{2j}} \frac{\partial^2}{\partial z^2}\frac{1}{R_{2ij}} dv'_j \Bigg].\end{aligned} \tag{22}$$

On the right-hand side of Equation 21 and Equation 22, the three integrals have the same form of derivatives of the gravitational potential produced by the jth prism and image prism. The first integral corresponds to the $\alpha-$component of the gravitational attraction produced by the jth prism. The second and third integrals correspond, respectively, to the $\alpha-$component of the gravitational attraction and to the $\alpha\, z-$component of the gravitational gradient tensor produced by the jth image prism. The similarity between the displacement fields due to a volume source in a half-space and the gravitational field allows the use of closed expressions of the gravitational potential and its derivatives produced by the 3D right rectangular prism. We draw the readers' attention to the fact that Vasco and Johnson (1987) were the pioneer in taking the advantage of the similarity between the displacement fields due to a source in a half-space and the gravitational field to calculate the displacement field due to a 2D volume source at the Earth surface. Here, our approach also takes the advantage of this similarity, but it calculates the displacement field due to a 3D volume source at the whole subsurface. In Equation 21 and Equation 22, the integrals depending on first derivatives of $\frac{1}{R_{1ij}}$ have the following closed solutions (Nagy et al., 2000, 2002):

$$\int_{x_{1j}}^{x_{2j}}\int_{y_{1j}}^{y_{2j}}\int_{z_{1j}}^{z_{2j}} \frac{\partial}{\partial x}\frac{1}{R_{1ij}} dv'_j = \left|\left|\left| yL_z + zL_y - xT_{yz} \right|_{X_{1j}}^{X_{2j}} \right|_{Y_{1j}}^{Y_{2j}} \right|_{Z_{1j}}^{Z_{2j}}, \tag{23}$$

$$\int_{x_{1j}}^{x_{2j}}\int_{y_{1j}}^{y_{2j}}\int_{z_{1j}}^{z_{2j}} \frac{\partial}{\partial y}\frac{1}{R_{1ij}} dv'_j = \left|\left|\left| xL_z + zL_x - yT_{xz} \right|_{X_{1j}}^{X_{2j}} \right|_{Y_{1j}}^{Y_{2j}} \right|_{Z_{1j}}^{Z_{2j}}, \tag{24}$$

and

$$\int_{x_{1j}}^{x_{2j}}\int_{y_{1j}}^{y_{2j}}\int_{z_{1j}}^{z_{2j}} \frac{\partial}{\partial z}\frac{1}{R_{1ij}} dv'_j = \left|\left|\left| xL_y + yL_x - zT_{xy} \right|_{X_{1j}}^{X_{2j}} \right|_{Y_{1j}}^{Y_{2j}} \right|_{Z_{1j}}^{Z_{2j}}, \tag{25}$$

where all derivatives are computed with respect to the coordinates of the ith point (x_i, y_i, z_i), and $L_x = \ln(x+R)$; $L_y = \ln(y+R)$; and $L_z = \ln(z+R)$; $T_{yz} = \tan^{-1}\left(\frac{yz}{x\,R}\right)$; $T_{xz} = \tan^{-1}\left(\frac{xz}{y\,R}\right)$; and $T_{xy} = \tan^{-1}\left(\frac{xy}{z\,R}\right)$; $R = \sqrt{x^2+y^2+z^2}$. The integration limits in Equations (23) to (25) are

$$\begin{aligned} X_{1j} &= x_i - x_{1j}, \\ X_{2j} &= x_i - x_{2j}, \\ Y_{1j} &= y_i - y_{1j}, \\ Y_{2j} &= y_i - y_{2j}, \\ Z_{1j} &= z_i - z_{1j}, \quad \text{and} \\ Z_{2j} &= z_i - z_{2j}. \end{aligned} \tag{26}$$

The remaining integrals, in the right-hand side of Equation 21 and Equation 22, depend on first and second derivatives of $\frac{1}{R_{2ij}}$. These integrals are conducted over the volume v_{2j} of the jth image prism and have the following closed solutions (Nagy et al., 2000, 2002):

$$\int_{x_{1j}}^{x_{2j}}\int_{y_{1j}}^{y_{2j}}\int_{z_{1j}-2\,z_c}^{z_{2j}-2\,z_c} \frac{\partial}{\partial x}\frac{1}{R_{2ij}} dv'_j = \left|\left|\left| yL_z + zL_y - xT_{yz} \right|_{X_{1j}}^{X_{2j}} \right|_{Y_{1j}}^{Y_{2j}} \right|_{Z_{1j}}^{Z_{2j}}, \tag{27}$$

$$\int_{x_{1j}}^{x_{2j}}\int_{y_{1j}}^{y_{2j}}\int_{z_{1j}-2\,z_c}^{z_{2j}-2\,z_c} \frac{\partial}{\partial y}\frac{1}{R_{2ij}} dv'_j = \left|\left|\left| xL_z + zL_x - yT_{xz} \right|_{X_{1j}}^{X_{2j}} \right|_{Y_{1j}}^{Y_{2j}} \right|_{Z_{1j}}^{Z_{2j}}, \tag{28}$$

$$\int_{x_{1j}}^{x_{2j}}\int_{y_{1j}}^{y_{2j}}\int_{z_{1j}-2\,z_c}^{z_{2j}-2\,z_c}\frac{\partial}{\partial z}\frac{1}{R_{2ij}}dv'_j=\left|\left|\left|xL_y+yL_x-zT_{xy}\right|_{X_{1j}}^{X_{2j}}\right|_{Y_{1j}}^{Y_{2j}}\right|_{Z_{1j}}^{Z_{2j}}, \tag{29}$$

$$\int_{x_{1j}}^{x_{2j}}\int_{y_{1j}}^{y_{2j}}\int_{z_{1j}-2\,z_c}^{z_{2j}-2\,z_c}\frac{\partial^2}{\partial x\partial z}\frac{1}{R_{2ij}}dv'_j=\left|\left|\left|L_y\right|_{X_{1j}}^{X_{2j}}\right|_{Y_{1j}}^{Y_{2j}}\right|_{Z_{1j}}^{Z_{2j}}, \tag{30}$$

$$\int_{x_{1j}}^{x_{2j}}\int_{y_{1j}}^{y_{2j}}\int_{z_{1j}-2\,z_c}^{z_{2j}-2\,z_c}\frac{\partial^2}{\partial y\partial z}\frac{1}{R_{2ij}}dv'_j=\left|\left|\left|L_x\right|_{X_{1j}}^{X_{2j}}\right|_{Y_{1j}}^{Y_{2j}}\right|_{Z_{1j}}^{Z_{2j}}, \tag{31}$$

and

$$\int_{x_{1j}}^{x_{2j}}\int_{y_{1j}}^{y_{2j}}\int_{z_{1j}-2\,z_c}^{z_{2j}-2\,z_c}\frac{\partial^2}{\partial z\partial z}\frac{1}{R_{2ij}}dv'_j=\left|\left|\left|-T_{xy}\right|_{X_{1j}}^{X_{2j}}\right|_{Y_{1j}}^{Y_{2j}}\right|_{Z_{1j}}^{Z_{2j}}. \tag{32}$$

In these integrals related to the jth image prism (Equations (27) to (29)), the integration limits along the z direction are given by

$$Z_{1j}=z_i-z_{1j}+2\,z_{cj}\text{ and }Z_{2j}=z_i-z_{2j}+2\,z_{cj}, \tag{33}$$

where $z_{cj}=\frac{1}{2}(z_{1j}+z_{2j})$ is the center depth of the jth prism. The remaining limits along x and y directions are the same defined by Equation 26.

The discrete stress forward modeling due to a reservoir in a homogeneous elastic semi-infinite medium

By following the similar approach used in the previous subsection, the stress field of each prism assuming constant pressure is calculated by an integrating solution for a nucleus of strain (Equation 15, Equation 16, and Equation 17) over its volume. This integration leads to a stress vector $\tilde{\boldsymbol{\sigma}}_{ij}\equiv\tilde{\boldsymbol{\sigma}}(x_i,y_i,z_i,x'_j,y'_j,z'_j)$ given by

$$\tilde{\boldsymbol{\sigma}}_{ij}=\iiint_{v_{1j}}\boldsymbol{\sigma_1}_{ij}dv'_j+\iiint_{v_{2j}}\boldsymbol{\sigma_2}_{ij}dv'_j, \tag{34}$$

where the first and second integrals are conducted, respectively, over the volumes v_{1j} and v_{2j} of the jth prism and the jth image prism. The total stress vector at the ith coordinates (x_i,y_i,z_i) due to the pressure change in the whole reservoir is calculated by the sum of all stress vector $\tilde{\boldsymbol{\sigma}}_{ij}$ (Equation 34), i.e.,

$$\tilde{\boldsymbol{\sigma}}_i=\sum_{j=1}^{M}\tilde{\boldsymbol{\sigma}}_{ij}\,. \tag{35}$$

By substituting Equation 16 and Equation 17 into Equation 34, we obtain the $\alpha-$component (where $\alpha=x$ and y) and the $z-$ component of the stress vector $\tilde{\boldsymbol{\sigma}}_{ij}$ as follows:

$$\tilde{\sigma}_{ij_\alpha}=A\Delta p_j\left[\iiint_{v_{1j}}\frac{\partial^2}{\partial\alpha\partial z}\frac{1}{R_{1ij}}dv'_j+\iiint_{v_{2j}}\frac{\partial^2}{\partial\alpha\partial z}\frac{1}{R_{2ij}}dv'_j+2z_i\iiint_{v_{2j}}\frac{\partial^3}{\partial\alpha\partial z^2}\frac{1}{R_{2ij}}dv'_j\right] \tag{36}$$

and

$$\tilde{\sigma}_{ij_z}=A\Delta p_j\left[\iiint_{v_{1j}}\frac{\partial^2}{\partial z^2}\frac{1}{R_{1ij}}dv'_j+\iiint_{v_{2j}}\frac{\partial^2}{\partial z^2}\frac{1}{R_{2ij}}dv'_j+2z_i\iiint_{v_{2j}}\frac{\partial^3}{\partial z^3}\frac{1}{R_{2ij}}dv'_j\right]. \tag{37}$$

Similarly to the displacement field (Equation 21 and Equation 22), the three integrals in the right-hand side of Equation 36 and Equation 37 have the same form of derivatives of the gravitational potential produced by the jth prism and image prism. The integrals depending on $\frac{1}{R_{1ij}}$ have the following closed solutions (Nagy et al., 2000, 2002):

$$\int_{x_{1j}}^{x_{2j}}\int_{y_{1j}}^{y_{2j}}\int_{z_{1j}}^{z_{2j}}\frac{\partial^2}{\partial x\partial z}\frac{1}{R_{1ij}}dv'_j=\left|\left|\left|L_y\right|_{X_{1j}}^{X_{2j}}\right|_{Y_{1j}}^{Y_{2j}}\right|_{Z_{1j}}^{Z_{2j}}, \tag{38}$$

$$\int_{x_{1j}}^{x_{2j}}\int_{y_{1j}}^{y_{2j}}\int_{z_{1j}}^{z_{2j}}\frac{\partial^2}{\partial y\partial z}\frac{1}{R_{1ij}}dv'_j=\left|\left|\left|L_x\right|_{X_{1j}}^{X_{2j}}\right|_{Y_{1j}}^{Y_{2j}}\right|_{Z_{1j}}^{Z_{2j}}, \tag{39}$$

and

$$\int_{x_{1j}}^{x_{2j}}\int_{y_{1j}}^{y_{2j}}\int_{z_{1j}}^{z_{2j}}\frac{\partial^2}{\partial z\partial z}\frac{1}{R_{1ij}}dv'_j=\left|\left|\left|-T_{xy}\right)\right|_{X_{1j}}^{X_{2j}}\right|_{Y_{1j}}^{Y_{2j}}\right|_{Z_{1j}}^{Z_{2j}}, \tag{40}$$

where the limits X_{1j}, X_{2j}, Y_{1j}, Y_{2j}, Z_{1j}, and Z_{2j} are defined by Equation 26. The integrals depending on second derivatives of $\frac{1}{R_{2ij}}$ in the right-hand side of 36 and Equation 37 have closed solutions defined by Equation 30, Equation 31, and Equation 32. Finally, the remaining integrals depending on third derivatives of $\frac{1}{R_{2ij}}$ have closed solutions given by (Nagy et al., 2000, 2002):

$$\int_{x_{1j}}^{x_{2j}}\int_{y_{1j}}^{y_{2j}}\int_{z_{1j}-2\,z_c}^{z_{2j}-2\,z_c}\frac{\partial^3}{\partial x\partial z^2}\frac{1}{R_{2ij}}dv'_j=\left|\left|\left|\frac{-yz}{R}\left(\frac{1}{x^2+z^2}\right)\right|_{X_{1j}}^{X_{2j}}\right|_{Y_{1j}}^{Y_{2j}}\right|_{Z_{1j}}^{Z_{2j}}, \tag{41}$$

$$\int_{x_{1j}}^{x_{2j}}\int_{y_{1j}}^{y_{2j}}\int_{z_{1j}-2\,z_c}^{z_{2j}-2\,z_c}\frac{\partial^2}{\partial y\partial z^2}\frac{1}{R_{2ij}}dv'_j = \left|\left|\left|\frac{-xz}{R}\left(\frac{1}{y^2+z^2}\right)\right|_{X_{1j}}^{X_{2j}}\right|_{Y_{1j}}^{Y_{2j}}\right|_{Z_{1j}}^{Z_{2j}}, \tag{42}$$

and

$$\int_{x_{1j}}^{x_{2j}}\int_{y_{1j}}^{y_{2j}}\int_{z_{1j}-2\,z_c}^{z_{2j}-2\,z_c}\frac{\partial^3}{\partial z^3}\frac{1}{R_{2ij}}dv'_j = \left|\left|\left|\frac{xy}{R}\left(\frac{1}{x^2+z^2}+\frac{1}{y^2+z^2}\right)\right|_{X_{1j}}^{X_{2j}}\right|_{Y_{1j}}^{Y_{2j}}\right|_{Z_{1j}}^{Z_{2j}}, \tag{43}$$

where the limits X_{1j}, X_{2j}, Y_{1j}, and Y_{2j} are defined by Equation 26 and Z_{1j} and Z_{2j} by Equation 33. Our method was implemented in Python programming language and it is based on Harmonica (Uieda et al., 2020). The horizontal and vertical displacements are calculated by using the volume integrations (Equation 21 and Equation 22), whose solutions are given by equations Equations (23) to (32). The horizontal and vertical stresses are calculated by using the volume integrations (Equation 36 and Equation 37), whose solutions are given by Equations (38) to (43). We used Fukushima (2020) to overcome the zero division in evaluating the arguments of the arctangent function.

NUMERICAL APPLICATIONS

Disk-shaped reservoir under uniform depletion

Embedded in a semi-infinite homogeneous medium, we simulated a vertical cylinder-like reservoir (not shown) with a radius of 500 m and whose horizontal coordinates of its center along the north-south and east-west directions are 0 m and 0 m, respectively. The depths to the top and to the bottom of the simulated reservoir are 750 m and 850 m, respectively. The reservoir is uniformly depleted by $\Delta p = -10$ MPa. The Young's modulus is 3300 (in MPa), the Poisson's coefficient is 0.25, and the uniaxial compaction coefficient C_m (Equation 12) is $2.2525\,10^{-4}$ MPa^{-1}. To apply our methodology, we discretized the cylinder along the $x-$ and $y-$ directions into a 20×20 grid of prisms. Hence, we totalized 400 prisms all of them centered at 800 m deep, with depths to the top and to the bottom at 750 m and 850 m and with pressure change Δp_j, $j = 1, ..., 400$ equal to -10 MPa. To apply the Geertsma's method (Geertsma, 1973), we used the disk-shaped reservoir described in Fjær et al. (2008) with dimensions and physical properties defined above. Figures 2 and 3 show cross-sections at $x = 0$ m of the displacement fields in 2D contour plots due to the pressure change in the whole cylindrical reservoir by using our methodology and Geertsma's method, respectively. As we defined the $z-$axis as positive downwards, the positive vertical displacement means a subsidence and the negative vertical displacement means an uplift. Figure 2 shows the horizontal and vertical displacements calculated, respectively, with Equation 20 and Equation 22 by our methodology. Figure 3 shows the radial and vertical displacements using Geertsma's method considering an elastic homogeneous cylindrical reservoir under uniform depletion based on the nucleus-of-strain concept in the half-space. In both cases (Figure 2b and Figure 3b) the vertical displacements due to the entire disk-shaped reservoir display a subsidence (positive values) above the reservoir and an uplift (negative values) below the reservoir. We stress that the proposed volume integrations (Equations (23) to (32) allowed to evaluate the vertical displacement (Figure 2b) throughout the entire reservoir. Rather, the vertical displacement using Geertsma's method (Figure 3b) is only valid outside the reservoir. The radial displacement using Geertsma's method (Figure 3a) shows positive values at the edges of the reservoir ($y = -500$ and $y = 500$) with a singularity at the center of the reservoir ($x = 0$, $y = 0$ and $z = 800$ m). The horizontal displacement with the proposed full integration (Figure 2a) shows positive values at the edges of the reservoir ($y = -500$ and $y = 500$); however, it does not present singularities inside the reservoir. Figure 4 shows the $x-$component displacement and the vertical displacement by our methodology that uses a full volume integrations. These displacements are calculated along the $x-$axis, at $y = 0$ m, and considering four surfaces located at the following depths: seafloor ($z = 0$ m), reservoir top ($z = 750$ m), reservoir center ($z = 800$ m) and reservoir bottom ($z = 850$ m). In the x-component of the displacement (Figure 4a), we can note an increased horizontal contraction from the center of the reservoir ($x = 0$) toward the reservoir edge ($x = 500$ m) where the maximum contraction of all surfaces occur. In the vertical displacement (Figure 4b), we can note a subsidence of the seafloor and the reservoir top (positive values) and an uplift of the reservoir bottom (negative values). The vertical displacements of the seafloor, the top and bottom of the reservoir for Geertsma's method (Figure 5) show similar behavior to those obtained by our methodology that uses full volume integrations (Figure 4b). However, we note that the subsidence of the seafloor is more attenuated in the Geertsma's method than in ours because we calculate the total displacement field outside and inside of the reservoir. This fact is important because the movement of the seafloor should be monitored in hydrocarbon fields under production. Figure 6 shows the null stress through the free surface at the plane $z = 0$ m due to the reservoir under uniform depletion.

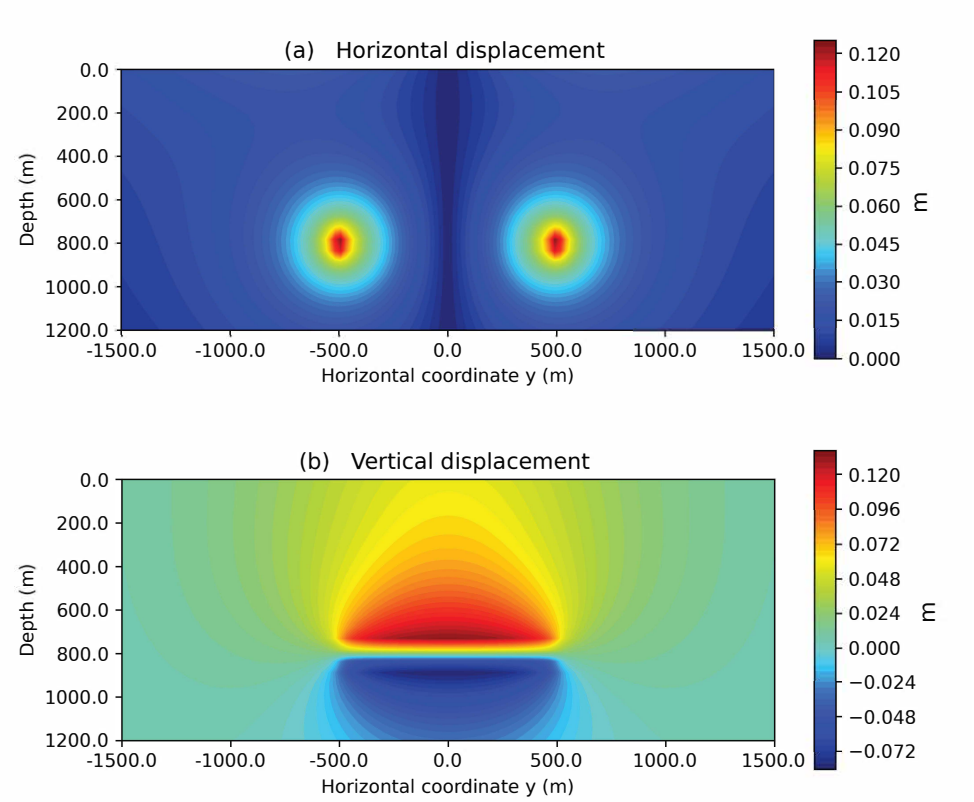

Figure 2: Reservoir under uniform depletion: (a) horizontal displacement (Equation 20) and (b) vertical displacement (Equation 22) by our methodology that uses the closed expressions of the volume integrations (Equation 21 and Equation 22), whose closed solutions are given by Equations (23) to (32).

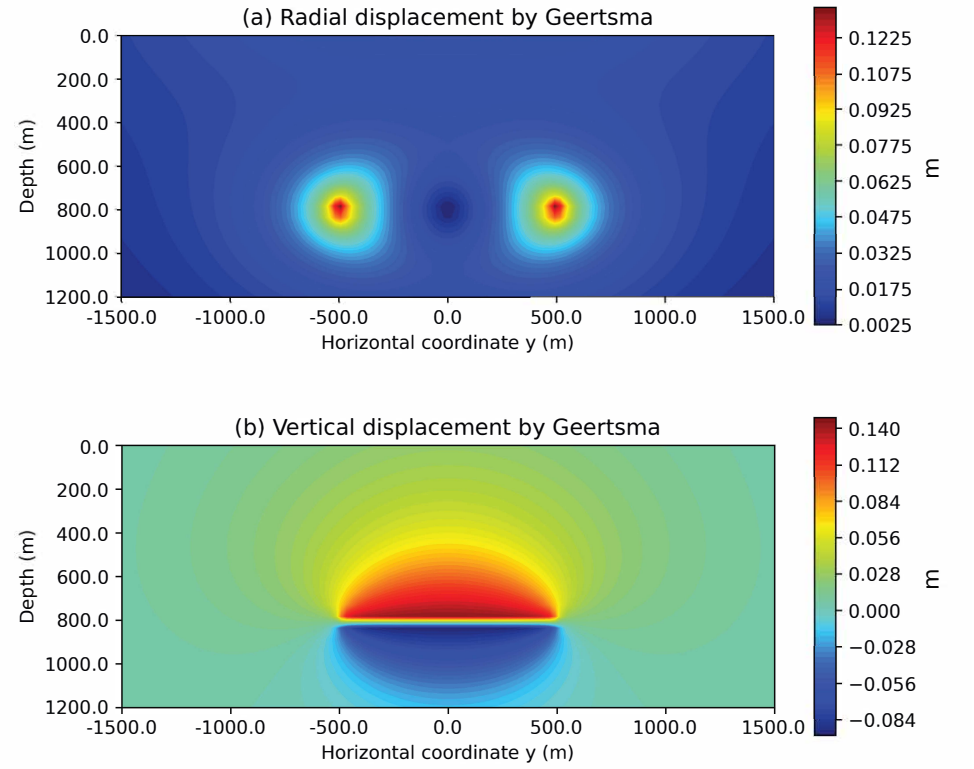

Figure 3: Reservoir under uniform depletion: (a) radial displacement and (b) vertical displacement using Geertsma's method (Geertsma, 1973) considering an elastic homogeneous cylindrical reservoir under uniform depletion (Fjær et al., 2008).

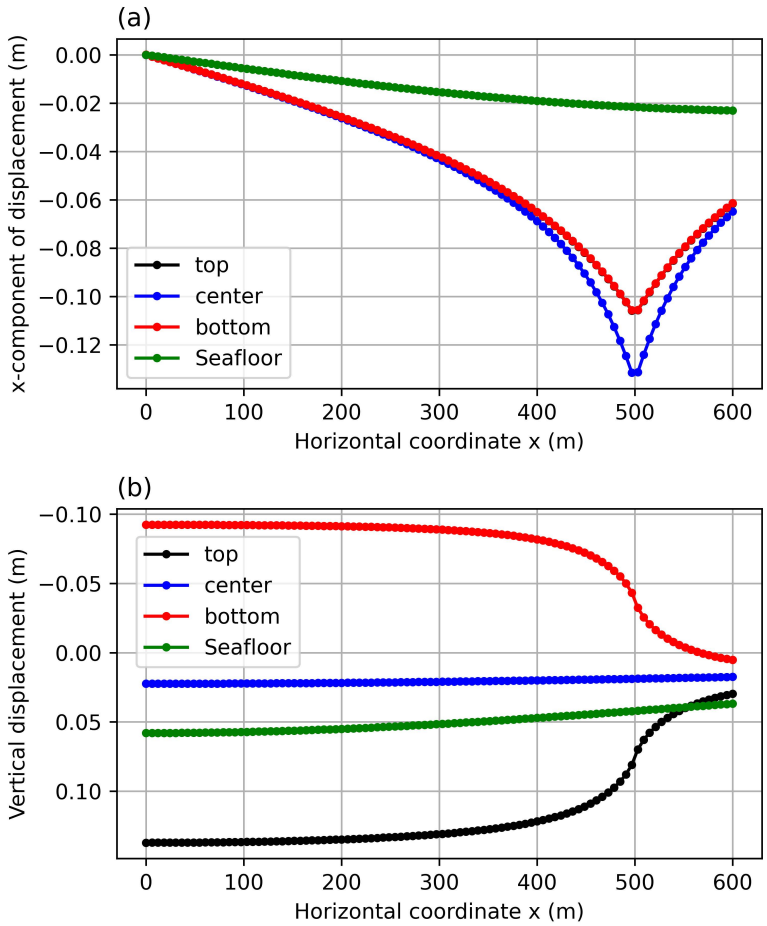

Figure 4: Reservoir under uniform depletion: (a) horizontal x-component displacement and (b) vertical displacement by our methodology that uses the closed expressions of the volume integrations (Equation 21 and Equation 22), whose closed solutions are given by equations Equations (23) to (32). These displacements are calculated along the x-axis, at $y = 0$ m and z located at the depths of: seafloor ($z = 0$ m), reservoir top ($z = 750$ m), reservoir center ($z = 800$ m) and reservoir bottom ($z = 850$ m).

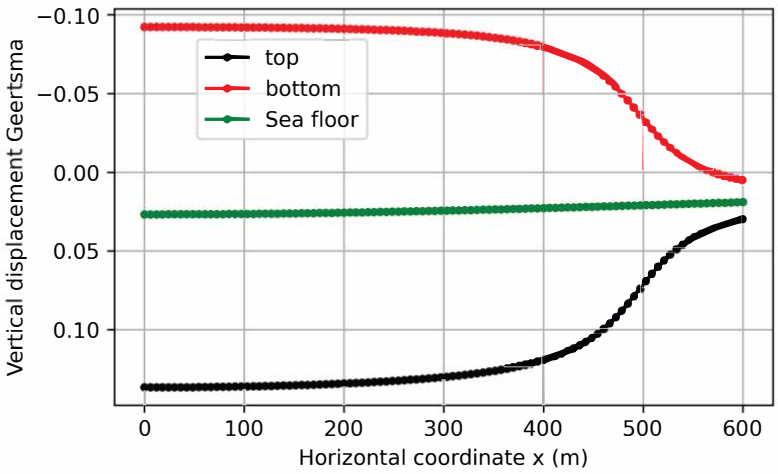

Figure 5: Reservoir under uniform depletion: vertical displacement using Geertsma's method (Geertsma, 1973) considering an elastic homogeneous cylindrical reservoir under uniform depletion (Fjær et al., 2008). The displacement is calculated along the x-axis, at $y = 0$ m and z located at the depths of: seafloor ($z = 0$ m), reservoir top ($z = 750$ m), and reservoir bottom ($z = 850$ m).

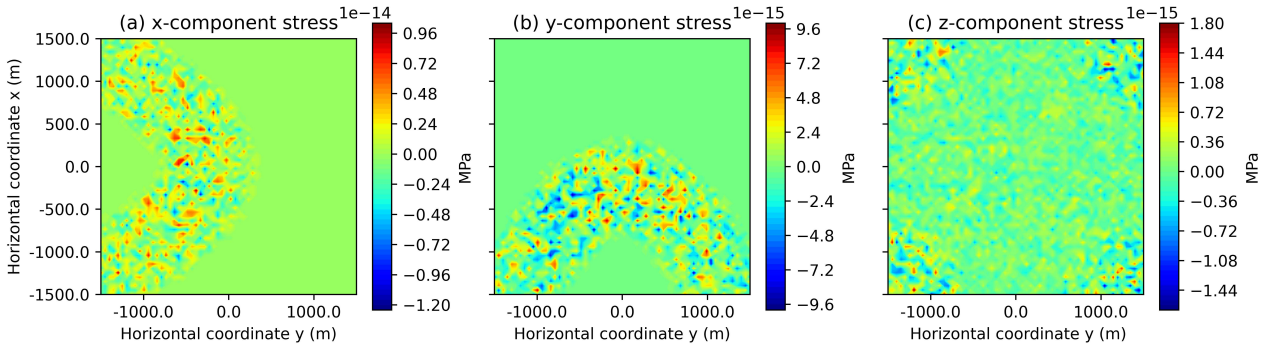

Figure 6: Reservoir under uniform depletion: (a) $x-$, (b) $y-$, and (c) $z-$components of the stress at the free surface. The horizontal and vertical stresses are calculated by using the full volume integrations (Equation 36 and Equation 37), whose closed solutions are given by equations Equations (38) to (43).

Reservoir with arbitrary geometry and under arbitrary pressure changes

In this numerical application, the reservoir model is a simplification of a realistic reservoir located in a production oil field in offshore Brazil. The entire reservoir model comprises dimensions of 14 km on the north-axis, 13 km on the east-axis, and 0.6 km on the down-axis. The depths to the top and bottom of the reservoir model are 2,712 m and 3,312 m, respectively. The components of the displacements are calculated at 0 m deep, on a regular grid of 100 × 80 observation points along the north- and east-directions, respectively. We discretized the reservoir along the $x-$, $y-$ and $z-$ directions into a $14\times13\times2$ grid of prisms. The Young's modulus is 3300 (in MPa), the Poisson's coefficient is 0.25, and the uniaxial compaction coefficient C_m (Equation 12) is $2.2525\,10^{-4}$ MPa^{-1}.

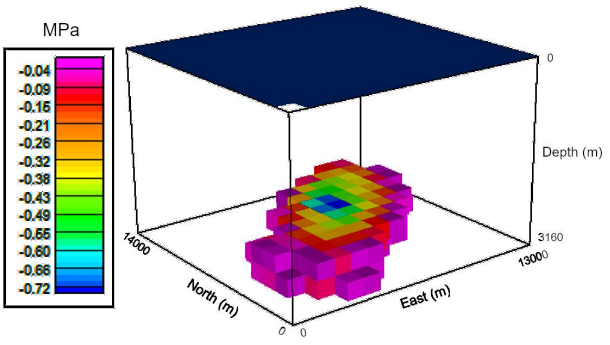

Figure 7: Reservoir with arbitrary geometry and under arbitrary pressure changes: 3D perspective view of the pore pressure distribution based on a reservoir located in a production oil field in offshore Brazil.

Figure 7 shows the pore pressure distribution of the reservoir whose pressures vary from 0 to −0.72 MPa. Figure 8 shows cross-sections at $x = 8$ km of the horizontal and vertical displacements, calculated in the whole reservoir by using our methodology. Figure 9 shows the null stress through the free surface due to reservoir shown in Figure 7.

CONCLUSION

Grounded on the similarity between the gravitational potential produced by a volume source under a density variation and the displacement field produced by a volume source in a half-space under a pressure variation, we have presented an alternative solution for the displacement and stress fields outside and inside of a 3D right rectangular prism with constant pressure change. Our solution is obtained by integrating the well-known nucleus-of-strain solution over the volume of the prism. We also use our solution to approximate the displacement and stress fields due to reservoir compaction with arbitrary geometry and under non-uniform pressure distribution. Our approach consists in approximating the reservoir 3D pressure distribution through a piecewise constant function defined on a user-specified grid of 3D prisms juxtaposed in the $x-$, $y-$, and $z-$directions. The sum of the displacements (stresses) produced by the prisms is the resultant displacement (stress) field due to the whole reservoir. Our expressions are valid either outside or inside the prisms. We have demonstrated the use of these expressions by applying them to calculate the displacement and stress fields due to cylindrical reservoirs with uniform and non-uniform pressure distributions and to a reservoir model of a production oil field in offshore Brazil. All the numerical applications produced null stress fields at the free surface showing that the condition of null tractions at the free surface has been met.

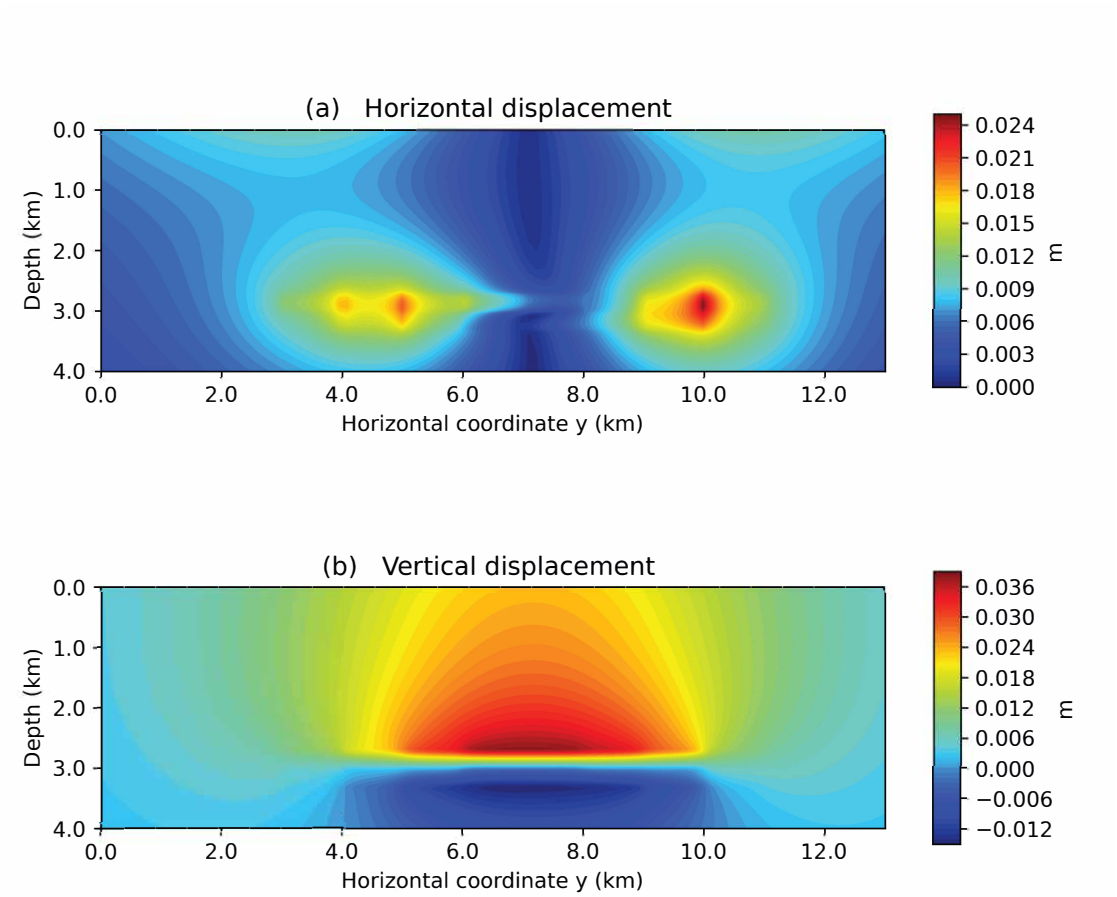

Figure 8: Reservoir with arbitrary geometry and under arbitrary pressure changes: (a) horizontal displacement (Equation 20) and (b) vertical displacement (Equation 22) by our methodology that uses the closed expressions of the volume integrations (Equation 21 and Equation 22), whose closed solutions are given by equations Equations (23) to (32).

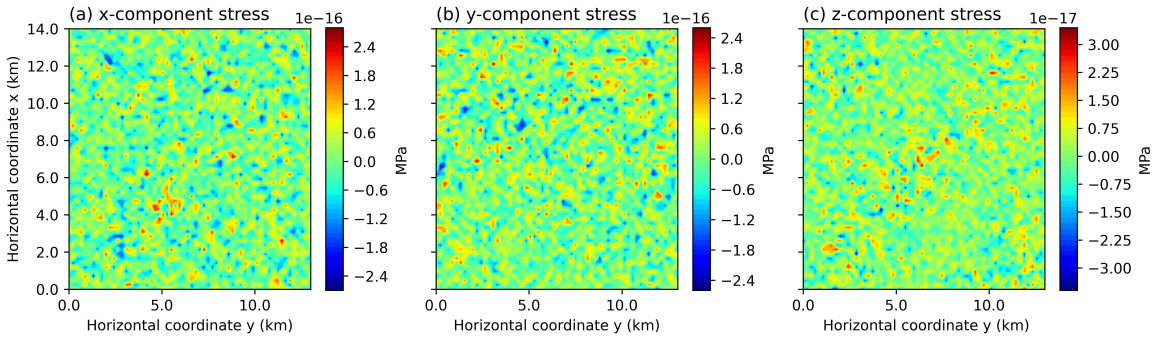

Figure 9: Reservoir with arbitrary geometry and under arbitrary pressure changes: (a) $x-$, (b) $y-$, and (c) $z-$components of the stress at the free surface. The horizontal and vertical stresses are calculated by using the full volume integrations (Equation 36 and Equation 37), whose closed solutions are given by equations Equations (38) to (43).

ACKNOWLEDGMENTS

We thank the editor George Sand L.A. de França and the reviewers for their criticisms and suggestions. Barbosa V.C.F. and Oliveira Jr V.C. were supported by fellowships from the Brazilian research agencies: CNPq (grants 309624/2021-5 and 315768/2020-7) and FAPERJ (grants E-26/202.582/2019 and E-26/202.729/2018). Arelaro A.D. and Borges F. thank PETROBRAS.

CODE AND DATA AVAILABILITY

The current version of our code is freely distributed under the BSD 3-clause license and it is available for download at Zenodo: https://doi.org/10.5281/zenodo.4041984. The latest development version of our code can be freely downloaded from a repository on GitHub (https://github.com/pinga-lab/DisReserv). Instructions for running the current version of our code are also provided on the repository. The code is still being improved and we encourage the user to work with the latest development version. The code was developed as an open-source Python language (Python 3.7.x). The numerical applications were produced in Jupyter Notebook. The data of the pore pressure distribution simulating a reservoir with arbitrary geometry and under arbitrary pressure changes (*realistic-model.pickle*) are available in the above-mentioned repositories.

REFERENCES

Beltrami, E., 1902–1920, Opere matematiche: Universitá di Roma, Facoltá Di Scienze, Italy.

Borges, F., M. Landrø, and K. Duffaut, 2020, Time-lapse seismic analysis of overburden water injection at the ekofisk field, southern north sea: Geophysics, **85**, B9–B21, doi: 10.1190/geo2019-0140.1.

Dahm, T., S. Cesca, S. Hainzl, T. Braun, and F. Krüger, 2015, Discrimination between induced, triggered, and natural earthquakes close to hydrocarbon reservoirs: A probabilistic approach based on the modeling of depletion-induced stress changes and seismological source parameters: Journal of Geophysical Research: Solid Earth, **120**, 2491–2509, doi: 10.1002/2014jb011778.

Fjær, E., R. M. Holt, P. Horsrud, A. M. Raaen, and R. Risnes., 2008, Petroleum related rock mechanics, developments in petroleum science, 2nd ed., v. 53 ed.: Elsevier.

Fukushima, T., 2020, Speed and accuracy improvements in standard algorithm for prismatic gravitational field: Geophysical Journal International, **222**, 1898–1908, doi: 10.1093/gji/ggaa240.

Geertsma, J., 1957, A remark on the analogy between thermoelasticity and the elasticity of saturated porous media: Journal of the Mechanics and Physics of Solids, **6**, 13–16, doi: 10.1016/0022-5096(57)90042-x.

Geertsma, J., 1966, Problems of rock mechanics in petroleum production engineering:: Proceedings of the First Congress of the International Society for Rock Mechanics, ISRM, Expanded Abstract, Lisbon, Portugal., **1**, 585–594.

Geertsma, J., 1973, Land subsidence above compacting oil and gas reservoirs: Journal of Petroleum Technology, **25**, 734–744, doi: 10.2118/3730-pa.

Geertsma, J., and van Opstal, 1973, A numerical technique for predicting subsidence above compacting reservoirs, based on the nucleus of strain concept: Verhandelingen Kon. Ned. Geol. Mijnbouwk. Gen., **28**, 63–78.

Goodiee, J., 1937, XCVII. On the integration of the thermo-elastic equations: The London, Edinburgh, and Dublin Philosophical Magazine and Journal of Science, **23**, 1017–1032, doi: 10.1080/14786443708561872.

Grigoli, F., S. Cesca, E. Priolo, A. P. Rinaldi, J. F. Clinton, T. A. Stabile, B. Dost, M. G. Fernandez, S. Wiemer, and T. Dahm, 2017, Current challenges in monitoring, discrimination, and management of induced seismicity related to underground industrial activities: A european perspective: Reviews of Geophysics, **55**, 310–340, doi: 10.1002/2016rg000542.

Kellogg, O. D., 1967, Foundations of potential theory, reprint from the first edition of 1929 ed.: Springer-Verlag, Berlin, Heidelberg.

Mehrabian, A., and Y. N. Abousleiman, 2015, Geertsma's subsidence solution extended to layered stratigraphy: Journal of Petroleum Science and Engineering, **130**, 68–76, doi: 10.1016/j.petrol.2015.03.007.

Mindlin, R. D., and D. H. Cheng, 1950, Thermoelastic stress in the semi-infinite solid: Journal of Applied Physics, **21**, 931–933, doi: 10.1063/1.1699786.

Muñoz, L. F. P., and D. Roehl, 2017, An analytical solution for displacements due to reservoir compaction under arbitrary pressure changes: Applied Mathematical Modelling, **52**, 145–159, doi: 10.1016/j.apm.2017.06.023.

Nagy, D., G. Papp, and J. Benedek, 2000, The gravitational potential and its derivatives for the prism: Journal of Geodesy, **74**, 552–560, doi: 10.1007/s001900000116.

Nagy, D., G. Papp, and J. Benedek, 2002, Corrections to "the gravitational potential and its derivatives for the prism": Journal of Geodesy, **76**, 475–475, doi: 10.1007/s00190-002-0264-7.

Segall, P., 1992, Induced stresses due to fluid extraction from axisymmetric reservoirs: Pure and Applied Geophysics, **139**, 535–560, doi: 10.1007/bf00879950.

Sen, B., 1951, Note on the stresses produced by nuclei of thermoelastic strain in a semi-infinite solid: Quarterly of Applied Mathematics, **8**, 365–369.

Sharma, B. D., 1956, Stresses in an infinite slab due to a nucleus of thermoelastic strain in it.: Zeitschrift

für Angewandte Mathematik und Mechanik, **36**, 75–78, doi: 10.1002/zamm.19560360108.

Tao, L., 1971, Integration of the dynamic thermoelastic equations: International Journal of Engineering Science, **9**, 489–505, doi: 10.1016/0020-7225(71)90050-4.

Tempone, P., E. Fjær, and M. Landrø, 2010, Improved solution of displacements due to a compacting reservoir over a rigid basement: Applied Mathematical Modelling, **34**, 3352–3362, doi: 10.1016/j.apm.2010.02.025.

Tempone, P., M. Landrø, and E. Fjær, 2012, 4d gravity response of compacting reservoirs: Analytical approach: Geophysics, **77**, G45–G54, doi: 10.1190/geo2010-0361.1.

Uieda, L., S. R. Soler, A. Pesce, V. C. Oliveira Jr, and N. Shea, 2020, Harmonica: Forward modeling, inversion, and processing gravity and magnetic data (v0.1.0): doi: 10.5281/zenodo.3628742.

van Thienen-Visser, K., and P. A. Fokker, 2017, The future of subsidence modelling: compaction and subsidence due to gas depletion of the groningen gas field in the netherlands: Netherlands Journal of Geosciences, **96**, s105–s116, doi: 10.1017/njg.2017.10.

Vasco, D. W., and L. R. Johnson, 1987, The correspondence between gravitational attraction and surface displacement due to volume expansion: Geophysical Journal International, **89**, 749–754, doi: 10.1111/j.1365-246x.1987.tb05191.x.

Barbosa, V.C.F. and Oliveira, Jr V.C.: study conception, mathematical deductions, Python codes; **Arelaro, A.D. and Barbosa, V.C.F.:** numerical applications; **All authors:** result analysis and interpretation, draft manuscript preparation, manuscript review, final manuscript approval.

Received on June 24, 2022 / Accepted on August 17, 2022